Macroscopic framework for viscoelasticity, poroelasticity and wave-induced flows – Part I: General Linear Solid

Igor B. Morozov and Wubing Deng

University of Saskatchewan, Saskatoon, Saskatchewan, CANADA,
E-mail: igor.morozov@usask.ca, wubing.deng@usask.ca

Abstract

Most field and laboratory observations of seismic wave propagation and attenuation are explained by using the viscoelastic (VE) model and effective moduli for rocks. This model is used to approximate most mechanisms of internal friction within materials including poroelasticity and wave-induced fluid flows (WIFF). However, the modulus-based viscoelasticity is still fundamentally different from pore-fluid effects. For example, wave attenuation in a poroelastic material is best described by a complex-valued effective density rather than by a VE modulus. In layered poroelastic medium, the VE approximation leads to incorrect predictions for the frequency-dependent Poisson's ratios and reflection coefficients. In heavy-oil compounds and media with WIFF, frictional forces should generally behave intermediately between the VE stresses and body-wave Darcy forces characteristic for poroelasticity. Thus, a broader theoretical framework is needed to incorporate the traditional viscoelasticity and poroelasticity and to extend them to broader WIFF models. Such a unified framework called the General Linear Solid (GLS) is proposed here. The GLS is a first-principle approach based on Lagrangian continuum mechanics, and it can be summarized as multiphase poroelasticity extended by solid and fluid viscosities. The formulation is carried out strictly in terms of measurable physical properties and boundary conditions from which the observable effects such as wave velocities and attenuation are predicted. Explicit differential equations are formulated in matrix form, from which a variety of numerical modeling schemes can be derived. In the GLS framework, the viscoelasticity represents an end-member characterized by zero Darcy-type friction, whereas the poroelasticity is an end-member with zero solid viscosity. Transitions between these end-members and their extensions yield new models such as 'visco-poroelasticity' and poroelasticity with multiple saturating fluids. The approach is illustrated on practical models of layered poroelastic and visco-poroelastic media. Applications of this framework are continued in Part II of this study.

Introduction

Reservoir rocks are heterogeneous, porous media saturated with potentially complex combinations of fluids and gases. When heavy oil is included in the saturation, the distinction between solid and fluid properties of the compound may become complicated or even completely blurred. Pore-flow effects become intertwined with solid and fluid viscosity, so that neither the poroelastic nor viscoelastic models alone provide accurate descriptions of the physics of seismic wave propagation. In this two-part paper (for Part II, see Morozov and Deng, submitted to *Geophysics*), we propose a formulation integrating both of these models and providing transitions between them. This formulation, hereafter called the General Linear Solid (GLS), is only constrained by the macroscopic character, isotropy and linearity of mechanical interactions, and therefore it provides a common framework for describing a broad range of rocks in field and laboratory environments.

The notion of equivalent medium is commonly used for modeling the propagation and attenuation of seismic waves in media with complex microstructures. The GLS framework attempts generalizing two broad groups of approaches to macroscopic equivalent media:

1) Poroelastic and wave-induced fluid flow models (WIFF), in which a fluid filtrates through microscopic pores (Biot, 1962) or between 'mesoscopic' heterogeneities (for recent reviews, see Toms et al. (2006) and Müller et al. (2010)).). We are interested in macroscopic expressions of such models, such as the squirt flows being represented by imaginary shifts in the effective bulk modulus of the pore fluid (Gurevich et al, 2010; Mavko, 2013).

2) The broadly-defined, linear viscoelastic (VE) model based on no specific mechanism but empirical, complex-valued and frequency-dependent effective moduli including the quality factors (Q) (e.g., Knopoff, 1964). In fluid dynamics, a similar approach uses effective viscosities instead of the effective moduli (e.g., Debautt and Thomas, 2004). With regard to weak oscillatory motions in a seismic wave, these approaches are equivalent, and we do not differentiate between them here. Note that despite their breadth, VE models are still distinctly different from poroelastic and WIFF ones but are often used to approximate them (Geertsma and Smit, 1961; Carcione, 1998).

One of the key differences between the above groups is in the significance of the notion of the effective VE modulus, which is only an approximate, derived quantity for models 1) but the core concept for 2).

In this study, we consider questions that may sound paradoxical, given a large body of research utilizing the VE moduli: Is it always appropriate to attribute the effects of internal friction within rock to the effective moduli? For example, for poroelasticity

and diffusive waves in fluids, the effective complex density represents a better alternative to the VE modulus (Johnson et al., 1987; Dupuy and Stovas, 2014). Further, is a *single* P-wave modulus sufficient for interpretation? Do we need a more general model combining multiple effective moduli and densities?

The GLS framework answers the above questions by generalizing the poroelastic and VE models and allowing transitions between and extensions beyond them. Instead of debating between the complex-valued moduli, viscosities, or densities, we show how the mechanics of the medium can be described simply and compactly without such quantities. The unified approach also helps constructing and analyzing VE approximations for poroelasticity (Geertsma and Smit, 1961; Carcione, 1998).

Within the GLS rheology, the end-member models 1) and 2) above are clearly identified as limits of zero solid viscosity ($\boldsymbol{\eta} = \mathbf{0}$) or zero Darcy friction ($\mathbf{d} = \mathbf{0}$) specified in section *Approach*. These limits reflect a fundamental difference in the physical characters of internal friction in these models. In viscoelasticity, frictional stresses are caused by velocity gradients, and their tensor forms are analogous to those in viscosity and elasticity. By contrast, in poroelasticity and likely WIFF, the internal friction is caused by the relative velocities of the constituents of the mixture. The pore-fluid frictional force is a *body* force analogous to the effects of inertia, and this force does not reduce to VE stress tensors (Carcione, 1998). However, it appears that realistic rocks should likely possess both of these properties, and hence we can generally expect $\boldsymbol{\eta} \neq \mathbf{0}$ and $\mathbf{d} \neq \mathbf{0}$.

The GLS is a first-principle approach based on Lagrangian mechanics, thermodynamics, symmetry and linearity of interactions, and it can thus be viewed as an extension of Biot's model of poroelasticity. The approach is macroscopic, i.e. formulated in terms of quantities averaged over scales shorter than the characteristic seismic wavelengths (about a meter) but longer than the micro- (μm) and mesoscopic (crack-size, cm) scales of structural heterogeneity. Only the macroscopic scale is 'felt' by the waves at seismic frequencies. At the same time, the values and petrophysical meanings of macroscopic parameters are determined by the micro- and mesoscopic-scale structures.

As in most applications of continuum mechanics, all interactions within the GLS framework are instantaneous and described by differential equations (Landau and Lifshitz, 1986). This ensures causality and naturally leads to finite-difference, finite-element, spectral and other types of numerical simulations. All parameters of the medium are real-valued and (generally) time- and frequency-independent. Frequency-dependent properties such as empirical moduli, viscosities, permeability and tortuosity (Johnson et al., 1987) arise when considering specific solutions. This is the key difference from many current models, which are usually developed for harmonic waves and include frequency-dependent material properties up front. The Lagrangian approach clearly differentiates between the observed properties of the seismic waves (such as velocities and apparent attenuation) and those truly belonging to the material (such as its density, rigidity, and viscosity). Explicit separation of the elastic, viscous, and Darcy forces allows differentiation between various physical mechanisms.

The goal of this Part I is in presenting the GLS methodology (section *Approach*) and demonstrating its links with poroelasticity and viscoelasticity (section *Applications*). However, section *Examples* also makes two important practical points that are rarely noted. In the first example, we use the GLS formalism to derive poroelastic models for brine- and gas- saturated sandstone. We model the frequency-dependent, complex-valued reflectivity r^* from a contact between brine- and gas-saturated zones and show that this reflectivity *does not* equal the expression for reflectivity usually expected from a VE approximation:

$$r^* \neq r^*_{VE} \equiv \frac{Z^*_2 - Z^*_1}{Z^*_2 + Z^*_1}, \tag{1}$$

where $Z^*_{1,2} = \sqrt{\rho_{1,2} M^*_{1,2}}$ are the complex-valued impedances inferred from the P-wave moduli $M^*_{1,2}$ for the two zones. The frequency dependence and the phase of reflectivity r^* from a zone of high poroelastic Q^{-1} (i.e., containing pore gas) are *opposite* to those predicted by r^*_{VE}. Note that the expectations of $r^* = r^*_{VE}$ in relation 1 motivated some of the recent experiments with proxies of heavy oil (Lines et al., 2014).

Thus, reflection amplitudes in a layered poroelastic medium cannot be inferred from a single effective modulus or Q in each of its layers. The same observation should apparently hold for WIFF. In fact, it is hard to say for what realistic rock type the true reflectivity r^* would equal the viscoelastic r^*_{VE}. This observation is similar to the "common fallacy" noted by White (1986), which consisted in inferring the P-wave Q_P from laboratory measurements of Young's (Q_E) and shear Q-factors (Q_S) and the Poisson's ratio (ν) by using VE relations between the moduli:

$$\frac{(1-\nu)(1-2\nu)}{Q_P} = \frac{(1+\nu)}{Q_E} - \frac{2\nu(2-\nu)}{Q_S}. \tag{2}$$

Unfortunately, this fallacy is still broadly encountered today. White (*ibid*) urged researchers "to recognize the losses due to simple fluid viscosity", i.e. to use first-principle models when interpreting the data on extensional deformations of rock samples.

In the second example, we illustrate the behavior of a more general, 'visco-poroelastic' material combining both poroelastic and VE properties. This model should be relevant to porous rock saturated with heavy oil, although the appropriate values of physical parameters are still poorly known.

Applications of the GLS model are continued in Part II, where we discuss the "homeogenization" (construction of macroscopic models from micro- and meso-structural ones), mixing and fluid-substitution relations for GLS media consisting of multiple constituents. It is shown that an equivalent 1-D WIFF medium formed by interlayered brine-and gas-saturated layers (Gurevich et al., 1997; Pride and Berryman, 2003; Müller and Gurevich, 2004) can be approximated by a visco-poroelastic

model. Finally, a VE model broadly used for simulating attenuation in seismic waveform modeling software (the Generalized Standard Linear Solid; e.g., Zhu et al., 2013) is also extended by using the GLS point of view (Part II).

Effective moduli, effective densities, Darcy friction, or GLS?

Comparisons of wave-propagation and attenuation models with observations are commonly based on measuring or modeling the effective VE moduli (e.g., Rubino and Holliger, 2012). These moduli represent the observed phase velocities and *Q*-factors of plane P- and S waves combined in complex-valued phase velocities: $V^*_{\mathrm{P,S}} \equiv V_{\mathrm{P,S}}\left[1 - i/\left(2Q_{\mathrm{P,S}}\right)\right]$, which are further combined with the density, ρ:

$$M^*_{\mathrm{eff}} \equiv \rho V^{*2}_{\mathrm{P}} \text{ and } \mu^*_{\mathrm{eff}} \equiv \rho V^{*2}_{\mathrm{S}}. \tag{3}$$

The use of complex moduli is inspired by the VE theory predicting characteristic frequencies in the absorption spectra of the several standard linear solids, Andrade, or Cole-Cole models (e.g., Geertsma and Smit, 1961; Lakes, 2009; Mavko, 2013). Poroelasticity can also be approximated by VE (e.g., Geertsma and Smit, 1961; Carcione, 1998), but this approximation is limited to modeling the spectra of $V_{\mathrm{phase}}(\omega)$ and $Q^{-1}(\omega)$ *in the primary wave mode* and *in a uniform space*. In a non-uniform poroelastic medium, VE attributes such as the dynamic moduli and *Q* do not behave "viscoelastically." To see this, note that treating the quantity M^*_{eff} in relations 3 as a "P-wave modulus" implies that it is also related to the Young's modulus E^*_{eff} and the Poisson's ratio ν^*_{eff} as in elasticity:

$$M^*_{\mathrm{eff}} = \mu^*_{\mathrm{eff}} \frac{4\mu^*_{\mathrm{eff}} - E^*_{\mathrm{eff}}}{3\mu^*_{\mathrm{eff}} - E^*_{\mathrm{eff}}}, \text{ and } M^*_{\mathrm{eff}} = E^*_{\mathrm{eff}} \frac{1 - \nu^*_{\mathrm{eff}}}{\left(1 + \nu^*_{\mathrm{eff}}\right)\left(1 - 2\nu^*_{\mathrm{eff}}\right)}. \tag{4}$$

These relations are often used to derive the M^*_{eff} from E^*_{eff}, μ^*_{eff} and ν^*_{eff} measured in laboratory experiments (Tisato and Madonna, 2012; Spencer, 2013; Batzle et al., 2014). However, both relations 4 can be modeled and turn out to be false for a poroelastic rod (White, 1986; Morozov, submitted to *Geophysical Journal International*). Phenomenologically, the reason for this discrepancy is that in poroelasticity (section *Applications* below), the complex-valued velocities in equations 3 are achieved through complex effective densities $\rho^* = \rho + i\rho'$ and not through the effective moduli.

Although the limitations of VE approximations to uniform media are well known in poroelasticity (e.g., Carcione, 1998), the effective-modulus paradigm is broadly used in practical studies. Adopting this paradigm leads to many significant implications. Describing wave attenuation by effective moduli allows extrapolating the Gassmann-type fluid substitution to nonzero frequencies (e.g., Makarynska et al., 2010; Mavko, 2013). By contrast, if we assume frequency-dependent effective densities, fluid-substitution equations for them should be different. Upscaling and averaging the effective densities would also lead to dramatically different models of equivalent media. Relations 4

between the different moduli would no longer be automatic, and the values of M, Q_P, K, and Q_K reported from laboratory experiments would change. Additional effects of the effective density would be in its frequency dependence, differences between the densities required to model P and S waves, and similar undesirable consequences. The VE-moduli paradigm is also instrumental for the theories of dynamic Poisson's ratios (Tschoegl et al., 2002; Lakes and Wineman, 2006).

Thus, neither by itself nor as an approximation, the VE model covers the variability of internal friction in realistic solids. We therefore need a more general formulation that could encompass the VE, poroelastic, and possibly WIFF models and allow transitions and comparisons between them.

Approach

In this section, we describe a broad class of linear rheologic laws that we call the General Linear Solid (GLS). This class contains the Newtonian fluid, models of saturated porous rock (Biot, 1962; Bourbié et al., 1987), their VE approximations (Carcione, 1998), and also all of the conventional VE models. The formulation also includes the models of linear solid viscosity used in earlier studies of wave attenuation (Ricker, 1941; Kolsky, 1963; Ben Menahem and Singh, 1981) and acoustic attenuation in metals (Landau and Lifshitz, 1986).

The key point of this approach is that since most of the dynamic variables within a composite medium are coupled, the density, elastic moduli, as well as the internal-friction properties should be represented by matrix quantities. The matrix character of inertial, elastic, and pore-fluid effects is recognized in poroelasticity (Bourbié et al., 1987; Pride and Berryman, 2003), and we only extend it to include the solid viscosity and potentially larger numbers of constituents.

With the use of the Lagrangian formalism and real-valued physical quantities, the above difficulties of preferring the complex moduli over complex densities or determining the mutual relations between the moduli disappear. A correspondence principle similar to that in conventional viscoelasticity (Ben Menahem and Singh, 1981; Lakes, 2009) can still be constructed. This principle also attains a matrix form, in which the VE effects are described by the imaginary parts of effective moduli, and the poroelastic and (likely) WIFF effects are replaced by imaginary effective densities. The resulting model is rigorous, allows transitions between the poroelastic and VE cases, and naturally extends to more complex media with multiple internal degrees of freedom. In the following subsections, we describe the key elements of the theory.

Lagrangian continuum mechanics with energy dissipation

The Lagrangian formalism is one of the most powerful and productive approaches to the mechanics of continuous media (Landau and Lifshitz, 1986). Because of its origin in the Hamiltonian variational principle, the Lagrangian approach greatly simplifies the mathematical formulation. This approach starts by identifying the relevant macroscopic

variables describing the deformation of the medium. For fluid or solid substitution in a porous medium, such variables are the volume fractions of the respective constituents and optionally other quantities that yet remain to be determined: areas of capillary solid-fluid contacts, statistical averages of heterogeneity, thicknesses of viscous boundary layers, etc.. These state variables are called the 'generalized coordinates,' and their time derivatives become the generalized velocities.

The dynamics of an elastic medium is completely described by specifying the Lagrangian density as a function of the generalized coordinates and velocities. Note that the coordinates and velocities are considered independent, and therefore deformations not satisfying the wave equations are also considered. For a linear and isotropic medium, the Lagrangian density is a combination of three scalar, second-order, rotational and translational invariants: the squared velocity $\dot{u}_i\dot{u}_i$ and two invariants of the strain tensor: $I_1^2 = (\varepsilon_{kk})^2$ and $I_2 = \varepsilon_{ij}\varepsilon_{ij}$. Two useful forms for this function are (e.g., Landau and Lifshitz, 1986; Aki and Richards, 2002):

$$L\{\mathbf{u},\dot{\mathbf{u}}\} = \frac{\rho}{2}\dot{u}_i\dot{u}_i - \frac{\lambda}{2}\varepsilon_{kk}\varepsilon_{ll} - \mu\varepsilon_{ij}\varepsilon_{ij} \equiv \frac{\rho}{2}\dot{u}_i\dot{u}_i - \frac{K}{2}\Delta^2 - \mu\tilde{\varepsilon}_{ij}\tilde{\varepsilon}_{ij}, \tag{5}$$

where $i = 1$, 2, or 3 denotes the spatial dimensions, ε_{ij} is the strain tensor, $\Delta \equiv \varepsilon_{kk} \equiv \mathrm{tr}\,\boldsymbol{\varepsilon}$ is the volumetric strain, $\tilde{\varepsilon}_{ij} \equiv \varepsilon_{ij} - \Delta\delta_{ij}/3$ is the deviatoric (pure shear) strain, and summations over all pairs of repeated indices are assumed. Parameters λ and μ are the Lamé constants, $K \equiv \lambda + 2\mu/3$ is the bulk modulus, and ρ is the mass density. All medium parameters (ρ, λ, K and μ) are real-valued and constrained by relations $\rho > 0$, $K \geq 0$, and $\mu \geq 0$, which guarantees non-negative elastic and kinetic energies (*ibid*). To describe a fluid, we only need to set $\mu = 0$.

The internal mechanical friction (due to fluid or solid viscosity) is described by a similar function called the dissipation function or pseudo-potential, D. Unlike the elastic energy, D principally depends on the velocities and strain rates. If we assume no internal variables (such as pore fluids) and linear internal friction, then similarly to expression 5, the dissipation function can only depend on the quadratic invariants of $\dot{\boldsymbol{\varepsilon}}$ (*ibid*):

$$D\{\mathbf{u},\dot{\mathbf{u}}\} = \frac{\eta_\lambda}{2}\dot{\Delta}^2 + \eta_\mu\dot{\varepsilon}_{ij}\dot{\varepsilon}_{ij} \equiv \frac{\eta_K}{2}\dot{\Delta}^2 + \eta_\mu\dot{\tilde{\varepsilon}}_{ij}\dot{\tilde{\varepsilon}}_{ij}. \tag{6}$$

This viscosity law ('rheology') leads to the Navier-Stokes equations for a Newtonian (compressible) fluid or to linear viscosity in a solid.

The General Linear Solid rheology

The construction of the GLS model can be viewed as a generalization of the matrix form of poroelasticity (Bourbié et al., 1987). Consider a mechanical continuum with N variables. The first of these variables will normally be the observable displacement $\mathbf{u}$ of the material, whereas others can be the volume fractions of pore fills or

some other displacement-like properties. Similarly to equations 5 and 6, consider the following second-order forms for the Lagrangian and dissipation function:

$$\begin{cases} L = \frac{1}{2}\dot{\mathbf{u}}_i^T \boldsymbol{\rho} \dot{\mathbf{u}}_i - V, \\ D = \frac{1}{2}\dot{\mathbf{u}}_i^T \mathbf{d} \dot{\mathbf{u}}_i + \frac{1}{2}\dot{\boldsymbol{\Delta}}^T \boldsymbol{\eta}_K \dot{\boldsymbol{\Delta}} + \dot{\tilde{\boldsymbol{\varepsilon}}}_{ij}^T \boldsymbol{\eta}_\mu \dot{\tilde{\boldsymbol{\varepsilon}}}_{ij}, \end{cases} \tag{7}$$

where V is the elastic-energy density:

$$V = \frac{1}{2}\boldsymbol{\Delta}^T \mathbf{K} \boldsymbol{\Delta} + \tilde{\boldsymbol{\varepsilon}}_{ij}^T \boldsymbol{\mu} \tilde{\boldsymbol{\varepsilon}}_{ij}, \tag{8}$$

and all matrix products are evaluated in the N-dimensional model space. In these equations, $\boldsymbol{\rho}$ is the density matrix, $\mathbf{K}$ and $\boldsymbol{\mu}$ are the elastic moduli matrices, $\boldsymbol{\eta}_K$ and $\boldsymbol{\eta}_\mu$ are the corresponding viscosity matrices, and $i,j = 1,2,3$ denote the spatial coordinates. An additional 'damping' matrix $\mathbf{d}$ is included in $\mathbf{D}$ based on the invariant $\dot{u}_i \dot{u}_i$, by analogy with the kinetic energy in L. This term represents the strain-unrelated mechanical friction that may (and therefore also should) arise between the different components of the system. Matrices $\boldsymbol{\rho}$, $\mathbf{K}$, $\boldsymbol{\mu}$, $\mathbf{d}$, $\boldsymbol{\eta}_K$, and $\boldsymbol{\eta}_\mu$ should be symmetric in the space of state variables. As in equation 5, each of these matrices should be positive definite. Translational invariance of the model (Galileo's principle) also requires that the element d_{11} of matrix $\mathbf{d}$ equals zero. Because one of the matrices $\boldsymbol{\rho}$, $\mathbf{d}$, and $\boldsymbol{\eta}$ can be diagonalized by selecting the internal variables, model 7 contains $(N+1)(5N/2+6)-1$ independent mechanical parameters.

To complete the general description of the model, note that the moduli $\mathbf{K}$ and $\boldsymbol{\mu}$ are isothermal properties of the material (Landau and Lifshitz, 1986). In empirical theories, such moduli are often called 'relaxed' because they operate at the state of equilibrium (Lakes, 2009). However, moduli $\mathbf{K}$ and $\boldsymbol{\mu}$ contain no relaxation with time. Increased values of the effective (empirical) moduli observed in fast transient processes or in high-frequency oscillations represent the *apparent* stiffness resulting from the internal friction $\boldsymbol{\eta}$ and $\mathbf{d}$. Such effects are demonstrated in the following sections.

Equations of motion

The equations of motion for the displacement field are obtained from the Euler variational derivatives of functions 7 and 8 (Landau and Lifshitz, 1986):

$$\boldsymbol{\rho} \ddot{\mathbf{u}}_i = -\mathbf{d} \dot{\mathbf{u}}_i + \partial_j \boldsymbol{\sigma}_{ij}, \tag{9}$$

where the strain-related (elastic and viscous) stress tensor equals:

$$\boldsymbol{\sigma}_{ij} = \mathbf{K} \boldsymbol{\Delta} \delta_{ij} + 2\boldsymbol{\mu} \tilde{\boldsymbol{\varepsilon}}_{ij} + \boldsymbol{\eta}_K \dot{\boldsymbol{\Delta}} \delta_{ij} + 2\boldsymbol{\eta}_\mu \dot{\tilde{\boldsymbol{\varepsilon}}}_{ij}. \tag{10}$$

As in viscoelasticity (Kolsky, 1963), for harmonic waves, the elastic and viscous stresses in equation 10 can be combined, yielding the correspondence principle.

The general form of the Lagrangian 7 leads to an important observation about the GLS systems. Only for matrices $\boldsymbol{\rho}$ containing a single nonzero element ρ_{11}, the behavior of other variables with $J > 1$ can be eliminated from equations 9 and reduces to memory integrals in time (Deng and Morozov, 2013; also see the last subsection in *Applications*). However, this construction of the density matrix is hardly realistic. For less trivial density matrices, the internal variables interact spatially (through terms containing $\boldsymbol{\lambda}$, $\boldsymbol{\mu}$, $\boldsymbol{\eta}_\lambda$, and $\boldsymbol{\eta}_\mu$ in equation 7) and lead to additional wave modes analogous to Biot's slow P waves. Therefore, simply specifying some $Q(\omega)$ dependence at every spatial point and implementing it by a set of massless internal variables should generally be insufficient for describing an inelastic system. For example, on the boundaries of a GLS body, one has to also formulate boundary conditions for all variables u_J with $J = 1,\ldots, N$. This situation is well known in poroelasticity, in which boundary conditions for fluid flow are required in addition to the usual continuity of the displacement and stress.

Correspondence principle

The correspondence principle is the basis of the VE model (Kolsky, 1963; Ben Menahem and Singh, 1981). For a GLS rheology, this principle also holds but takes a different form that can be derived as follows. For a harmonic oscillation at angular frequency ω, all variables $\mathbf{u}$ are proportional to $\exp(-i\omega t)$, and consequently equations 9 and 10 can be written as an "equivalent" elastic problem:

$$\boldsymbol{\rho}^* \ddot{\mathbf{u}}_i = \partial_j \boldsymbol{\sigma}_{ij}, \text{ where } \boldsymbol{\sigma}_{ij} = \boldsymbol{\lambda}^* \boldsymbol{\Delta} \delta_{ij} + 2\boldsymbol{\mu}^* \boldsymbol{\varepsilon}_{ij}, \tag{11}$$

in which the (matrix) parameters of the medium are complex-valued and explicitly depend on ω:

$$\boldsymbol{\rho}^* \equiv \boldsymbol{\rho} + \frac{i}{\omega}\mathbf{d}, \ \boldsymbol{\lambda}^* \equiv \boldsymbol{\lambda} - i\omega\boldsymbol{\eta}_\lambda, \text{ and } \boldsymbol{\mu}^* \equiv \boldsymbol{\mu} - i\omega\boldsymbol{\eta}_\mu. \tag{12}$$

The replacement of viscosities $\left(-\omega\boldsymbol{\eta}_\lambda\right) \to \operatorname{Im}\boldsymbol{\lambda}^*$ and $\left(-\omega\boldsymbol{\eta}_\mu\right) \to \operatorname{Im}\boldsymbol{\mu}^*$ represents the VE correspondence principle. Note that the portion of the internal friction described by $\mathbf{d}$ modifies the *density* matrix $\boldsymbol{\rho}^*$, which becomes complex-valued (equation 12). This is fundamentally different from viscoelasticity, in which the density is always assumed to be real-valued (Anderson and Archambeau, 1964). Nevertheless, the case of $\mathbf{d} \neq \mathbf{0}$ and $\boldsymbol{\eta} = \mathbf{0}$ represents the essence of the poroelastic and likely WIFF models.

Wave modes

In this section, we derive the dispersion relations (frequency-dependent phase velocity and attenuation) for a uniform GLS medium. Consider a plane P wave in which

all spatial displacements are oriented in the direction of axis X: $u_{Jk} = u_J \delta_{k1}$, where the upper-case subscript '$_J$' enumerates model variables and the lower-case '$_k$' refers to the spatial coordinates. The strain equals $\varepsilon_{Jik} = u'_J \delta_{i1} \delta_{k1}$, where the prime denotes the spatial derivative in X. The equation of motion 9 then simplifies to:

$$\boldsymbol{\rho}\ddot{\mathbf{u}} = -\mathbf{d}\mathbf{u} + \mathbf{M}\mathbf{u}'' + \boldsymbol{\eta}_M \dot{\mathbf{u}}'', \tag{13}$$

where $\mathbf{M} \equiv \mathbf{K} + 4\boldsymbol{\mu}/3$ is the (matrix) P-wave modulus and $\boldsymbol{\eta}_M \equiv \boldsymbol{\eta}_K + 4\boldsymbol{\eta}_\mu/3$ is the P-wave viscosity.

Further, let the wave be harmonic in time:

$$\mathbf{u} = \mathbf{A} \exp\left(-i\omega t + ikx - \alpha x\right), \tag{14}$$

where A_J is the amplitude (including the relative phase shift) of the J^{th} variable, ω is the frequency, k is the wavenumber, and α is the damping factor (logarithmic spatial decrement of the amplitude). Denoting $\gamma \equiv \left(k + i\alpha\right)^2 / \omega^2$, equation 13 shows that the wave modes $\boldsymbol{\upsilon}^{(n)}$ and the corresponding $\gamma^{(n)}$ can be obtained from the following generalized eigenvector problem:

$$\boldsymbol{\rho}^* \boldsymbol{\upsilon}^{(n)} = \gamma^{(n)} \mathbf{M}^* \boldsymbol{\upsilon}^{(n)}. \tag{15}$$

where $\mathbf{M}^* \equiv \mathbf{M} - i\omega\boldsymbol{\eta}_M$ is the complex matrix P-wave modulus as in equations 12.

The eigenvector problem 15 has normally N eigenvectors corresponding to the P-wave modes existing in this medium. For example, in poroelasticity (next section), $N = 2$, and the eigenvectors represent the primary and Biot's secondary P waves. From the corresponding values of γ, the phase velocity of the wave is obtained:

$$V_{\text{phase}} \equiv \omega/k = 1/\operatorname{Re}\sqrt{\gamma}, \tag{16a}$$

and the energy dissipation factor, defined as $Q^{-1} \equiv \alpha/(2k)$:

$$Q^{-1} = \operatorname{Im}\sqrt{\gamma} \Big/ \left(2 \operatorname{Re}\sqrt{\gamma}\right). \tag{16b}$$

The dependences of these V_{phase} and Q^{-1} on frequency are illustrated for poroelastic and GLS models in section *Examples* and for GSLS- and equivalent WIFF media in Part II.

With weak dissipation, for an eigenmode n satisfying equations 15 and 16, the kinetic and potential energies in equation 7 equal each other. This *energy equipartitioning* (also known as the Rayleigh principle; Aki and Richards, 2002) is useful for calculating the amount of dispersion and attenuation in heterogeneous media. As shown in Appendix A, for dominant $\boldsymbol{\eta}$- or $\mathbf{d}$-type friction, analogous equal-energy relations give estimates of skin depths and wave diffusivities.

Effective moduli

Since the effective moduli are broadly used in interpretation (e.g., Makarynska et al., 2010; Mavko, 2013), it is important to see how they fit in the GLS model. The meanings of effective moduli are nontrivial when diffusive waves and mesoscopic heterogeneity become significant (e.g., White, 1975; Dutta and Odé, 1979a; Pride and Berryman, 2003; Carcione and Picotti, 2006). As a practical aspect of these questions, consider whether it is sufficient to characterize the internal friction within a medium by only giving its Q (e.g. White, 1965, 1986; Lines et al., 2008, 2014; Tisato and Madonna, 2012; Spencer, 2013; Zhu et al., 2013).

Generally, with N internal variables in a GLS body, N effective moduli for each wave mode are required in order to describe its P-wave response. The *scalar*, empirical dynamic moduli represent averages of the combinations of $\boldsymbol{\rho}$, $\mathbf{K}$, $\boldsymbol{\mu}$, $\boldsymbol{\eta}_K$, $\boldsymbol{\eta}_\mu$, and $\mathbf{d}$ for the selected wave modes (Appendix A). Thus, scalar effective moduli are wave-mode dependent and may be difficult to relate to pure material properties. In contrast to the scalar modulus, a *matrix* effective bulk modulus $\mathbf{K}^*$ can always be defined for a material (equation 12). However, this effective modulus must be used together with the matrix effective density. Only taken together, these quantities contain all of the effects of the internal friction.

In summary, the use of effective moduli for describing material properties in poroelastic and GLS media with $N > 1$ can be either complicated or ambiguous and insufficient. In such cases, we recommend the direct use of the constitutive matrix properties $\boldsymbol{\rho}$, $\mathbf{K}$, $\boldsymbol{\mu}$, $\boldsymbol{\eta}_K$, $\boldsymbol{\eta}_\mu$, and $\mathbf{d}$, as illustrated in the following sections and Part II.

Applications

Equations 7–8 contain all of the standard VE and poroelastic models. In this section, we show how each of these models can be compactly solved in matrix GLS form.

Poroelasticity

With two variables ($N = 2$), zero viscosity ($\boldsymbol{\eta} = \mathbf{0}$), and appropriately selected matrices $\boldsymbol{\rho}$, $\mathbf{K}$, $\boldsymbol{\mu}$ and $\mathbf{d}$, equations 7 represent Biot's (1962) poroelasticity. To obtain the poroelastic case, we denote by $\mathbf{u}_1$ the observable deformation of the fluid-saturated rock. If the porosity ϕ is approximately constant, it is convenient to take the internal variable $\mathbf{u}_2$ as the filtration displacement (relative displacement between the fluid and its unperturbed position in host matrix) multiplied by ϕ: $\mathbf{u}_2 \equiv -\mathbf{w} \equiv -\phi\left(\mathbf{u}_{\text{fluid}} - \mathbf{u}_1\right)$. The relations for the solid stress tensor σ_{ij} and the pore pressure p follow from the volumetric potential V in relation 8:

$$\sigma_{ij} = \frac{\partial V}{\partial \varepsilon_{ij}}, \text{ and } \quad p = \frac{\partial V}{\partial \xi}, \tag{17}$$

where $\xi \equiv -\operatorname{div}\mathbf{w}$ is the fluid content. For an isotropic medium, V is given by the following quadratic form (section 2.2.2 in Bourbié et al., 1987):

$$V = \frac{1}{2}K_w\Delta^2 + \mu\tilde{\varepsilon}_{ij}\tilde{\varepsilon}_{ij} - \alpha M\Delta\xi + \frac{1}{2}M\xi^2 . \tag{18}$$

In our notation (expressions 7), the dilatational and deviatoric strains associated with the two displacement fields are $\Delta_1 \equiv \Delta$, $\Delta_2 \equiv \xi$, $\tilde{\varepsilon}_{1ij} \equiv \tilde{\varepsilon}_{ij}$, and $\tilde{\varepsilon}_{2ij} = 0$. Therefore, relation 18 is the elastic part of the Lagrangian 7, with matrix moduli:

$$\mathbf{K} = \begin{bmatrix} K_U & -\alpha M \\ -\alpha M & M \end{bmatrix} \text{ and } \boldsymbol{\mu} = \begin{bmatrix} \mu & 0 \\ 0 & 0 \end{bmatrix}. \tag{19}$$

Here, K_U is the undrained bulk modulus of the system with constant fluid content ($\mathbf{u}_2 = 0$), and parameter M is the pressure that needs to be exerted on the fluid in order to increase the fluid content ξ by a unit value at constant volume (i.e., when $\Delta = 0$). Parameter $\alpha \in [0, 1]$ is the Biot-Willis coefficient measuring the proportion of the apparent dilatational strain caused by variations in fluid content. These parameters are related to the bulk modulus of drained rock frame, K_D, by: $\alpha^2 M = K_U - K_D$ (*ibid*).

The kinetic energy density in the poroelastic model equals (*ibid*):

$$E_{kin} = \frac{\rho}{2}\dot{u}_i\dot{u}_i + \rho_f\dot{u}_i\dot{w}_i + \frac{a\rho_f}{2\phi}\dot{w}_i\dot{w}_i , \tag{20}$$

where ρ_f is the density of the pore fluid, ϕ denotes the porosity, and $a \geq 1$ is the tortuosity of the pore space. This expression is again contained in the Lagrangian 7, with density matrix:

$$\boldsymbol{\rho} = \begin{bmatrix} \rho & -\rho_f \\ -\rho_f & \dfrac{a}{\phi}\rho_f \end{bmatrix}. \tag{21}$$

Biot's dissipation pseudo-potential equals $D = \eta\dot{w}_i\dot{w}_i/(2\kappa)$, where η is the pore-fluid viscosity and κ is the absolute permeability(*ibid*). This D corresponds to the following simple form of matrix $\mathbf{d}$ in equations 7:

$$\mathbf{d} = \begin{bmatrix} 0 & 0 \\ 0 & \eta/\kappa \end{bmatrix}. \tag{22}$$

Thus, the system of Biot's poroelastic equations represents a special case of the GLS model 7–9 in which $N = 2$ and $\boldsymbol{\eta} = \mathbf{0}$. Considering larger values of N and nonzero matrices $\boldsymbol{\eta}$ gives natural extensions of Biot's model to multiple pore fluids (below) and

visco-poroelasticity (section *Examples*).

Poroelasticity with two fluids

Several authors considered poroelasticity with two filtration fluids. These models can be cast as GLS models with $N = 3$. For example, Pride and Berryman (2003) derived equations governing the linear acoustics of composites consisting of two poroelastic constituents. Their approach involved averaging Biot's differential equations of motion with boundary conditions to produce linear equations for the equivalent macroscopic deformation field. This model can be compactly written in the form of relations 7, with $N = 3$ corresponding to one macroscopic frame and two pore flows. Note that Pride and Berryman's (2003) equations were obtained in three key steps (equations 28, 33, 40, and 43 in that paper): 1) averaging the time derivative of the macroscopic energy, $\langle \dot{E} \rangle$, 2) relating $\langle \dot{E} \rangle$ to the derivatives of an effective strain-energy potential denoted R, and 3) presenting the stresses and momentum transport (Newton's equations) by matrix relations based on the second derivatives of R. These steps are close to spatial averaging (Appendix A) of the poroelastic GLS functions 7.

Pride and Berryman (2003) also suggested a reduction of their model to an equivalent Biot's model with a single pore fluid ($N = 2$) when one of the fluids is entirely embedded within the other ($\xi_3 \equiv \mathrm{div}\mathbf{u}_3 = \mathbf{0}$). The number of degrees of freedom in such an equivalent medium is a nontrivial problem considered in Part II. In the GLS formalism, this reduction can be performed in an elegant manner by using "Lagrange multipliers," or "source terms" for ξ_3 in the Lagrangian (Landau and Lifshitz, 1986).

Beresnev (2014) developed a quasi-static model for porous rock saturated with two nonviscous fluids with interfacial tension. His model was also based on linearity and quadratic invariants of strain tensors, and consequently it also belongs to the class of GLS models with $N = 3$. The equations for stresses in the solid and fluid phases were derived from the potential V in equation 8, which was defined similarly to equation 18. However, to achieve a single wave equation, Beresnev (*ibid*) additionally postulated that the volumetric deformations ($\xi \equiv \mathrm{div}\mathbf{u}$) were equal for all three phases, and assumed a mixing law combining the stresses within the phases in a common effective stress, σ. Among other simplifications, this modification led to requiring $\alpha = 0$ in the solid-fluid coupling terms in equation 18. This replaced the three-dimensional wave equation (with three eigenmodes in equation 15) with a scalar one, leading to a scalar effective P-wave modulus $M = \sigma/\xi$.

Another useful application of the case $N = 3$ is the model of rock containing 'soft' (compliant) and 'stiff' porosities (Mavko and Jizba, 1991). These two types of porosity differ in that only soft pores drain upon passage of a seismic wave. The amounts of the two porosities, ϕ_{soft} and ϕ_{stiff}, can vary with the imposed effective stress (*ibid*). In the GLS form, the difference between the fluids in stiff and soft pores can be described by the density and drag matrices:

$$\boldsymbol{\rho} = \begin{bmatrix} \rho & \rho_f & \rho_f \\ \rho_f & \dfrac{a_{\text{stiff}}}{\phi_{\text{stiff}}}\rho_f & 0 \\ \rho_f & 0 & \dfrac{a_{\text{soft}}}{\phi_{\text{soft}}}\rho_f \end{bmatrix} \text{ and } \mathbf{d} = \begin{bmatrix} 0 & 0 & 0 \\ 0 & \eta/\kappa_{\text{stiff}} & 0 \\ 0 & 0 & \eta/\kappa_{\text{soft}} \end{bmatrix}, \tag{23}$$

with variables u_2 and u_3 being the volume fractions of fluids occupying the stiff and soft pores, respectively. The low mobility of fluids in stiff pores suggests that $\eta/\kappa_{\text{stiff}} \gg \eta/\kappa_{\text{soft}}$ and possibly $a_{\text{stiff}}/\phi_{\text{stiff}} \gg a_{\text{soft}}/\phi_{\text{soft}}$. Large values of d_{22} and ρ_{22} 'freeze' the fluid within stiff pores at high (ultrasonic) frequencies, creating the apparent 'unrelaxed' effective modulus and faster wave velocities discussed by Mavko and Jizba (*ibid*).

Viscoelastic solids

Inelastic solids (in a broad sense, as media dissipating mechanical energy during deformation) are often modeled by "viscoelastic (VE) solids." Frictional forces within VE solids are combined with elastic stresses and attributed to time-dependent VE moduli (Lakes, 2009). The time-dependent moduli are often implemented by mathematical 'memory variables' (e.g., Carcione, 1998) or by mechanical systems such as the well-known linear solids (Liu et al., 1976; Carcione, 2007; Lakes, 2009).

All VE solids implementable by mechanical systems belong to the GLS rheologies. Examples of such models are the commonly used Maxwell, Kelvin-Voigt, Burgers, and the Generalized Standard Linear Solid (GSLS). Note that spring-dashpot arrangements such as shown in Figures 1 and 2 can be viewed as diagrams of the construction of the GLS Lagrangian and dissipation function (equations 7 and 8). To describe the deformation of a Maxwell solid, we need to use the usual observable displacement $\mathbf{u}_1 \equiv \mathbf{u}$ plus one internal variable $\mathbf{u}_2$ connecting the elastic and damping elements (Figure 1a). Therefore, the material-parameter matrices in relations 7 contain two rows and two columns:

$$\boldsymbol{\rho} = \begin{bmatrix} \rho & 0 \\ 0 & 0 \end{bmatrix}, \ \mathbf{M} = \begin{bmatrix} M & -M \\ -M & M \end{bmatrix}, \text{ and } \boldsymbol{\eta} = \begin{bmatrix} 0 & 0 \\ 0 & \eta \end{bmatrix}, \tag{24}$$

where the modulus $\mathbf{M}$ (M) denotes any type of the viscoelastic (elastic) moduli, and η denotes the damping element in Figure 1a. The form of the elastic matrix $\mathbf{M}$ shown in equations 24 corresponds to the strain (for example, shear) energy equal $\mu\left(\tilde{\varepsilon}_{1ij} - \tilde{\varepsilon}_{2ij}\right)\left(\tilde{\varepsilon}_{1ij} - \tilde{\varepsilon}_{2ij}\right) = \mu\tilde{\varepsilon}_{1ij}\tilde{\varepsilon}_{1ij} - 2\mu\tilde{\varepsilon}_{1ij}\tilde{\varepsilon}_{2ij} + \mu\tilde{\varepsilon}_{2ij}\tilde{\varepsilon}_{2ij}$ (Figure 1a). Note that this matrix resembles the matrix $\mathbf{M}$ in poroelasticity (equation 19), although it is much simpler and singular ($\det\mathbf{M} \equiv 0$).

For a Kelvin-Voigt solid (Figure 1b), there are no internal variables, and the corresponding 1×1 constitutive matrices are:

$$\boldsymbol{\rho} = [\rho],\ \mathbf{M} = [M], \text{ and } \boldsymbol{\eta} = [\eta]. \tag{25}$$

The GSLS (which is the Standard Linear solid with $N = 2$) is constructed by using $L \equiv N - 1$ internal (or memory) variables (usually, $L = 5$ or 6 in finite-difference modeling; Zhu et al., 2013). The GLS matrices for this solid are (Figure 2):

$$\boldsymbol{\rho} = \begin{bmatrix} \rho & 0 & 0 & \cdots & 0 \\ 0 & 0 & 0 & \cdots & 0 \\ 0 & 0 & 0 & \ddots & 0 \\ \vdots & \vdots & \ddots & \ddots & \vdots \\ 0 & 0 & 0 & \cdots & 0 \end{bmatrix},\ \mathbf{M} = \begin{bmatrix} \sum_{J=1}^{N} M_J & -M_2 & -M_3 & \cdots & -M_N \\ -M_2 & M_2 & 0 & \cdots & 0 \\ -M_3 & 0 & M_3 & \ddots & 0 \\ \vdots & \vdots & \ddots & \ddots & \vdots \\ -M_N & 0 & 0 & \cdots & M_N \end{bmatrix}, \tag{26a}$$

$$\text{and } \boldsymbol{\eta} = \begin{bmatrix} \eta_1 & 0 & \cdots & 0 \\ 0 & \eta_2 & 0 & 0 \\ \vdots & 0 & \ddots & 0 \\ 0 & 0 & 0 & \eta_N \end{bmatrix}. \tag{26b}$$

The values of M_J and η_J are usually selected to achieve $Q^{-1}(\omega) \approx const$ within the frequency band of interest (*ibid*).

Thus, all practical linear VE solids belong to the GLS rheology. At the same time, a comparison of the matrices 24 and 26 for VE models with those for poroelasticity (equations 21 and 22) reveals that the VE case is only a narrow subset of the GLS, with a quite specific construction:

1) The VE model disregards the direct 'drag' friction (matrix **d** = **0)** caused by the differential velocities of the variables.
2) This model ignores the inertia of all secondary constituents and also the kinematic coupling between them, which reduces the matrix **ρ** to a single nonzero element. This appears to be the most restrictive assumption. By contrast, realistic physical systems always exhibit inertial effects.
3) The GSLS model also ignores the elastic coupling between all of its Maxwell bodies (Figure 2). As a result, the modulus matrix **M** is sparse and contains only N nonzero values out of possible $N(N+1)/2$.

The sparsity of matrices **ρ** and **M** (relation 26) and **d** = **0** in a GSLS suggests that significantly more general effects can be expected from a similar set of internal variables. Some of these effects are examined in Part II.

Examples

For realistic quantitative examples, consider a high-porosity, brine- and gas-saturated rock with parameters by Dutta and Odé (1979b) (Table 1). These parameters correspond to young, unconsolidated Texas Gulf Coast sand near 1600-m depths. Gas parameters correspond to methane at these depths. Also following Dutta and Odé (*ibid*), we set the tortuosity equal one and disregard the frequency dependence of the dynamic viscosity and permeability. We use the poroelastic parameterization of the preceding section ($N = 2$) extended with solid viscosity. For uniform gas- and brine-saturated layers, the phase velocities and Q^{-1} for the primary and secondary P waves obtained from equation 15 are shown in Figure 3. In the examples below, we model the reflections and mode conversions of these wave modes at the boundary of these layers by using the propagator-matrix method (Appendix B).

Reflections from a contrast in attenuation

Reflections from "Q contrasts" such as gas-saturated zones attracted significant interest in early studies of seismic attenuation (e.g., Lockett, 1962; White, 1965; Cooper and Reiss, 1966; Bourbié and Nur, 1984). Recently, this interest was revived in the studies of heavy oil (Lines et al., 2008; Wong and Lines, 2013; Lines et al., 2014). It was noted that reflections from a zone of increased Q^{-1} should be phase-shifted (Lines et al., 2008). However, Morozov (2011b) also pointed out a significant uncertainty about the magnitude and even the sign of this phase shift. The derivations based on the VE theory (i.e., using r^*_{VE} in equation 1) predict a negative imaginary shift of the normal-incidence reflection coefficient from a low-Q medium (Lines et al., 2014):

$$r^* \approx \frac{\Delta Z - i\,Z/(2Q)}{2Z} = r\big|_{Q^{-1}=0} - \frac{i}{4Q}, \tag{27}$$

where $Z \equiv \rho V$ is the conventional acoustic impedance and ΔZ is its small contrast between the two media, and it is assumed that $Q \gg 1$. This prediction implies that by means of the complex modulus $\left(M^*_{\text{eff}}\right)$, the "attenuation" produces forces acting on the boundary of the two media. Forces of such kind could come from viscosity. However, in a poroelastic medium, the surface stress (equation 10) is elastic and the Darcy's friction (represented by matrix **d** in equation 9) is a body force. Such body-force friction does not act on the boundary, and consequently a positive sign of Imr^* can be expected (Lines et al., 2008; Morozov, 2011):

$$r^* \approx r\big|_{Q^{-1}=0} + \frac{i}{4Q}. \tag{28}$$

At the same time, poroelasticity requires an additional condition on the fluid flow across the boundary. This boundary condition affects the value of r^*, and consequently, the values of Q^{-1} for the two media do not contain the information necessary for evaluating

the r^*.

To model the r^* in Biot's poroelasticity, consider a boundary between brine- and gas-saturated sandstone layers (Table 1). This problem was solved by Dutta and Odé (1983), and by taking advantage of the matrix formulation, we give a different form of this solution in Appendix B. The reflection and mode-conversion coefficients for an incident primary P wave are contained in the first column of matrix **R** (Appendix B). These coefficients are shown in Figure 4b and compared to the r^*_{VE} derived by using the VE formula 1 (Figure 4a). The exact poroelastic solution and its VE approximation are similar for frequencies below the absorption peaks (about 10^4 Hz; Figure 3b), but above the peaks, the r^* and r^*_{VE} diverge strongly. Note that $\mathrm{Im} r^* > 0$ at all frequencies (Figure 4b), whereas $\mathrm{Im}\, r^*_{VE}$ is predominantly negative (Figure 4a).

Thus, the VE approximation does not accurately predict the reflectivity in a layered porous, fluid-saturated medium. The differences between the predictions by the exact poroelastic model and its VE approximation are of the same magnitude as the total variation of the reflectivity with frequency (Figure 4). These differences are due to the secondary P waves. Because of their strong attenuation, secondary P waves are not observed within long wave paths within uniform media, but they are present near reflecting boundaries, with amplitudes strongly variable with frequency and angles of incidence (Dutta and Odé, 1983). Similarly, secondary waves strongly affect the moduli and Q^{-1}s measured in cylindrical rock samples in the laboratory (White, 1986; Morozov, submitted to *Geophysical Journal International*).

Visco-poroelasticity

In the second example, we add the effects of rock and fluid viscosity to the poroelastic predictions (Figure 3). It is likely that along with Darcy's filtration-flow friction, the porous rock frame also exhibits some viscous friction. A popular approach to modeling such friction consists in making the drained and undrained moduli in relations 19 complex-valued, with frequency dependences corresponding to one or several Standard Linear Solids (Mavko, 2009). Carcione (1998) proposed phenomenological equations of motion for such a "poroviscoelastic" medium by constructing L memory variables to represent the GSLS for the rock frame (Figure 2) plus an additional memory variable for poroelastic relaxation. In the GLS form, this corresponds to using $N = L + 2$ variables, with matrices $\boldsymbol{\rho}$, $\mathbf{K}$, $\boldsymbol{\eta}$, and $\mathbf{d}$ combining those of the GSLS (equation 26) and poroelasticity (equations 19, 21, and 22). Similarly to relations 26, these matrices are large and sparse when $L > 0$. As argued above, this sparsity and massless variables can be viewed as physical drawbacks (although also mathematical advantages) of this model. Therefore, we try an opposite approach that we call "visco-poroelasticity", in which we simply add a solid-viscosity matrix $\boldsymbol{\eta}$ to Biot's poroelastic model with $N = 2$.

The values of solid viscosity for rocks are poorly known. Pride et al. (1992)

compiled estimates of bulk viscosity in fluids and gases showing that η_K can be 2.8–5 times larger than shear viscosity for water and brine, 2 times larger for air, about 150 times larger for hydrocarbons, and about 450 times larger for carbon dioxide. For a conservative estimate, let us take $\eta_M = \eta_K + 2\eta/3 \approx 5\eta$ as the bulk viscosity of brine and pore gas in our models (Table 1) and assume that this viscosity operates (macroscopically) within the pores similarly to its action in the free fluids. For rock, the viscosity (and particularly the bulk viscosity) is poorly known. Ricker (1941) estimated $\eta_M \approx 3.8 \cdot 10^6$ Pa·s ($3.8 \cdot 10^9$ cP) for sandstone; however this value included the mesoscopic effects of fluid-filled fractures. In global seismology, it is believed that $\eta_K \approx 0$ (in the form of $Q_K^{-1} \approx 0$) for most rocks (Anderson and Archambeau, 1964), although Knopoff (1964) also offered evidence to the contrary. To assess the likely range of rock viscosities, consider a diagonal bulk-viscosity matrix in equation 15:

$$\boldsymbol{\eta}_M = \begin{bmatrix} \eta_M & 0 \\ 0 & 5\eta_{\text{brine or gas}} \end{bmatrix}, \tag{29}$$

where we try an arbitrarily small value of $\eta_M = 0.1$Pa·s (100 cP) as well as Ricker's $\eta_M = 3.8 \cdot 10^6$ Pa·s ($3.8 \cdot 10^9$ cP). The results of this modeling are shown in panels c and d in Figures 5 and 6.

Even with a very weak solid viscosity of $\eta_M = 0.1$Pa·s, the behavior of the composite material changes significantly at higher frequencies (Figure 5a and b). Qualitatively, this behavior of $Q^{-1}(\omega)$ is similar to $Q_{\text{P}}^{-1}(\omega)$ measured in bitumen sands by Spencer (2013), although the variations of Q^{-1} there are located at lower frequencies, apparently because of much higher viscosity of the bitumen. The introduction of viscosities also dramatically changes the higher-frequency reflection coefficients (Figure 6a and b). As in the preceding section, the VE approximation incorrectly predicts the imaginary part of the reflection coefficient $r_{VE}^* \neq r^*$ as well as its variations with frequency.

For larger $\eta_M = 3.8 \cdot 10^6$ Pa·s, viscosity effects dominate the internal friction, and the GLS behaves as a Kelvin-Voigt solid up to about 300–1000 Hz (panels c and d in Figures 5 and 6). Above these frequencies, the dispersion and attenuation become unrealistically high (Figures 5c and d). At such frequencies (more precisely, strain rates) the viscosity should likely become nonlinear and effectively decrease with frequency (Coulman et al, 2013). Because the material is predominantly viscous, the VE approximation for reflectivity is in this case acceptable below frequencies of about 300–1000 Hz (compare Figures 6c and d), and conversions to secondary waves are extremely weak (gray lines in Figures 6d; note that their values are multiplied by 100 for plotting).

Above about 300–1000 Hz, significant differences are observed between the reflectivities r^* in the GLS solution and its VE approximation r_{VE}^* (Figures 6d and c, respectively). Thus, whenever a "poroelastic" effect is significant in a GLS model, the

reflectivity r_{VE}^{*} inferred by a VE approximation to it appears inaccurate.

Discussion

For a given *N*, relations 7 and 8 give (nearly) the most general form of functions *L* and *D* for a multiphase, linear isotropic medium. The only simplification made in this form is the absence of coupling between the macroscopic bulk ($\boldsymbol{\Delta}$) and shear ($\tilde{\boldsymbol{\varepsilon}}$) deformations. As shown above, because of such generality, the forms 7 and 8 contain the entire viscoelasticity and poroelasticity. Similarly, this general form should also contain macroscopic descriptions of WIFF mechanisms as long as they satisfy the criteria of isotropy and linearity, and a suitable value of *N* is determined (Part II).

The unified GLS approach offers substantial methodological benefits. The formulation is simple, expressed by instantaneous differential equations and is therefore automatically causal. By contrast, causality is a nontrivial issue for frequency-domain VE models (Aki and Richards, 2002). The focus on physical internal variables encourages specific, detailed analysis of the microstructure and of the processes of internal friction. The notions of elastic-energy density and dissipation rates are simple and directly correspond to the observed quantities (again unlike in VE, where they represent elaborate time-delayed integrals subject to significant uncertainties; see section 2.1 in Carcione (2007)). Relaxation of the moduli can be studied under specific experimental conditions and not assumed to be purely time-dependent. Finite-difference and other numerical algorithms directly follow from the equations of motion and mechanical variational principles. The averaging relations (Appendix A) lead to natural "homogenization" methods for heterogeneous media.

For practical applications, the simple GLS model 7–8 requires further development in several broad areas, such as: 1) nonlinearity and/or boundary layers to explain the dynamic elasticity, viscosity (Coulman et al., 2013), and permeability (Johnson et al., 1987), 2) explicit models for WIFF effects in various geometries of the microstructure, 3) capillary effects, and 4) thermodynamic effects. Although each of these topics requires extensive studies, they completely fit within the GLS framework, similarly to the full range of physical phenomena being captured by the Lagrangian formalism (see Landau and Lifshitz (1986) and other volumes of this classic series). Replacing empirical frequency-dependent parameters with explicit models based on matrix material properties and differential equations would allow closer insights into the physical character of deformations, fluid flows, and internal friction. Studies of such models are continued in Part II of this paper.

Conclusions

An extending of Biot's approach to fluid-saturated rock, solid/fluid viscosity, and matrix medium properties leads to a general linear macroscopic model for wave propagation in solids, fluids, and their mixtures. The model called the General Linear Solid (GLS) is only constrained by the mechanical principles of linearity, energy, and

isotropy. Due to such generality, the model incorporates all results from both poroelasticity and the conventional linear viscoelasticity and also allows combining the poroelastic and viscoelastic behaviors. Such combined properties should likely be present in porous rocks saturated with heavy oil and/or containing wave-induced fluid flows (WIFF). Because of its roots in mechanics, the model is free from the complexities of the viscoelastic model caused by the reliance on time-dependent material properties.

An application to poroelasticity shows that the frequency-dependent and phase-shifted reflectivity between poroelastic media disagrees with the predictions based on the conventional viscoelastic relations based on effective moduli. Therefore, for realistic media, the viscoelastic approximation may be problematic when analyzing heterogeneous media, such as in modeling seismic reflections or interpreting laboratory experiments with rock samples.

Acknowledgments

W. D. was supported by the Scholarship Council, P. R. China. This research was also supported by NSERC Discovery Grant RGPIN261610-03. GNU Octave software (http://www.gnu.org/software/octave/) was used for numerical modeling. Comments by two anonymous reviewers have greatly helped in improving the manuscript.

References

Aki, K. and Richards, P.G., 2002. Quantitative Seismology, Second Ed., University Science Books, Sausalito, California.

Anderson, D. L., and Archambeau, C. B., 1964. The anelasticity of the Earth: J. Geophys. Res.*,* **69**, 2071–2084.

Batzle, M. L., G. Kumar, R. Hoffmann, L. Duranti, and L. Adam (2014). Seismic-frequency loss mechanisms: Direct observations: The Leading Edge, 33, 656-662.

Ben-Menahem, A., and S. J. Singh (1981). Seismic waves and sources, Springer-Verlag

Beresnev, I., 2014. Compressional-wave propagation in porous media saturated with two fluids: Geophysics, **79** (1), L1–L11, doi: 10.1190/GEO2013-0200.1

Biot, M. A. 1962. Mechanics of deformation and acoustic propagation in porous media: J. Appl. Phys., **23**, 1482–1498

Bourbié, T., and Nur A., 1984. Effects of attenuation on reflections: Experimental test: J. Geophys., Res., **89** (B7), 6197-6202.

Bourbié, T., Coussy, O., and Zinsiger, B. 1987. Acoustics of porous media, Editions TECHNIP, France, ISBN 2-7108-0516-2

Carcione, J. M., 2007. Wave fields in real media: Wave propagation in anisotropic anelastic, porous, and electromagnetic media. Second Edition, Elsevier

Carcione. J. M., and S. Picotti, 2006. P-wave seismic attenuation by slow-wave diffusion: Effects of inhomogeneous rock properties: Geophysics 71(3), O1-O8, doi: 10.1190/1.2194512

Cooper, H. F., Jr., and Reiss, F. L., 1966. Reflection of plane viscoelastic waves from plane boundaries: J. Acoust. Soc. Am., **39**, 1133–1138.

Cooper, R., 2002. Seismic wave attenuation: Energy dissipation in viscoelastic crystalline solids, in: S.-I, Karato and H. R. Wenk (Eds.), Plastic deformation of minerals and rocks: Rev. Mineral Geochem., **51**, 253–290.

Dupuy, B., and A. Stovas, 2014. Influence of frequency and saturation on AVO attributes for patchy saturated rocks: Geophysics, **79** (1), B19–B36, doi: 10.1190/GEO2012-0518.1

Gurevich, B., Zyirianov, and S. L. Lopatnikov, 1997. Seismic attenuation in finely layered porous rocks: Effects of fluid flow and scattering: Geophysics, **62** (1), 319–324.

Gurevich, B., D. Makarynska, O. B. de Paula, and M. Pervukhina, 2010. A simple model for squirt-flow dispersion and attenuation in fluid-saturated granular rocks: Geophysics, 75 (6), N109–N120,doi: 10.1190/1.3509782

Coulman, T., Deng, W., and Morozov, I., 2013. Models of seismic attenuation measurements in the laboratory: Canadian J. Expl. Geoph, **38** (1), 51–67.

Debbaut, B., and K. Thomas, 2004. Simulation and analysis of oscillatory squeeze flow: J. Non-Newtonian Fluid Mech. **124**, 77–91

Deng, W., and Morozov, I. B., 2013, New approach to finite-difference memory variables by using Lagrangian mechanics: CSPG/CSEG/CWLS Convention, http://cseg.ca/resources/abstracts/2013-conference-abstracts-a-to-h, accessed Dec. 22, 2013

Dutta, N. C., and H. Odé, 1979a. Attenuation and dispersion of compressional waves in

fluid-filled porous rocks with partial gas saturation (White model)–Part I: Biot theory: Geophysics, **44** (11), 1777–1788.

Dutta, N. C., and H. Odé, 1979b. Attenuation and dispersion of compressional waves in fluid-filled porous rocks with partial gas saturation (White model)–Part II: Results: Geophysics, **44** (11), 1789–1805.

Dutta, N. C., and H. Odé, 1983. Seismic reflections from a gas-water contact, Geophysics, **48** (2), 148–162.

Geertsma, J., and D. C. Smit, 1961. Some aspects of elastic wave propagation in fluid-saturated porous solids: Geophysics, **26** (2), 161–181.

Johnson, D. L., J. Koplik, and R. Dashen, 1987. Theory of dynamic permeability and tortuosity in fluid-saturated porous media, J. Fluid Mech., **176**, 379–402.

Kennett, B. L. N., and Kerry, N. J., 1979, Seismic waves in a stratified half space: Geophys. J. Roy. Astr. Soc., **57**, 557–583.

Knopoff, L. 1964. *Q*: Rev. Geophys., **2**, 625–660.

Kolsky, H., 1963. Stress waves in solids, Dover Publications.

Lakes, R., 2009. Viscoelastic materials, Cambridge, ISBN 978-0-521-88568-3.

Lakes R.S., and Wineman, A., 2006. On Poisson's ratio in linearly viscoelastic solids: J Elasticity, **85**, 45–63

Landau L. D., and Lifshitz, E.M., 1986. Course of theoretical physics, volume 7 (3rd English edition): Theory of elasticity, Butterworth-Heinemann, ISBN 978-0-7506-2633-0

Landau L. D., and E. M. Lifshitz, 1987. Course of theoretical physics, volume 6: Fluid mechanics, (2nd English edition): Butterworth-Heinemann, ISBN 978-0-7506-2767-2

Lines, L., Vasheghani, F., and Treitel, S., 2008. Reflections on *Q*: CSEG Recorder, **33** (10), 36-38.

Lines, L., Wong, J., Innanen, K., Vasheghani, F., Sondergeld, C., Treitel, S., and Ulrych, T., 2014. Research Note: Experimental measurements of *Q*-contrast reflections: Geophysical Prospecting **62**, 190–195, DOI: 10.1111/1365-2478.12081

Liu, H. P., Anderson, D. L., and Kanamori, H., 1976. Velocity dispersion due to anelasticity: implications for seismology and mantle composition: Geophys. J. R. Astr. Soc., **47**, 41–58.

Lockett, F. J., 1962. The reflection and refraction of waves at an interface between viscoelastic media: J. Mech. Phys., Solids, **10**, 53-64.

Makarynska, D., B. Gurevich, J. Behura, and M. Batzle, 2010. Fluid substitution in rocks saturated with viscoelastic fluids: Geophysics, **75** (2), B115-122, doi: 10.1190/1.3360313.

Mavko, G., T. Mukerji, and J. Dvorkin, 2009. The rock physics handbook, 2nd ed.: Cambridge University Press.

Mavko, G., 2013. Relaxation shift in rocks containing viscoelastic pore fluids: Geophysics, 78, M19-M28, doi: 10.1190/GEO2012-0272.1

Mavko, G., and D. Jizba, 1991. Estimating grain-scale fluid effects on velocity dispersion in rocks: Geophysics, **56** (12), 1940-1949

Morozov, I. B., 2011. Anelastic acoustic impedance and the correspondence principle: Geophys. Prosp.: doi 10.1111/j.1365-2478.2010.00890.x

Morozov, I. B., Dynamic moduli and Poisson's ratios in experiments with fluid-saturated porous rock: Submitted to *Geophysical Journal International*

Morozov, I. B., and W. Deng Unified macroscopic model for viscoelasticity and wave-induced flow – Part II: Equivalent media: Submitted to *Geophysics*

Müller, T. M., and B. Gurevich, 2004, One-dimensional random patchy saturation model for velocity and attenuation in porous rocks: Geophysics, **69**, 1166–1172.

Müller, T., B. Gurevich, and M. Lebedev, 2010. Seismic wave attenuation and dispersion resulting from wave-induced flow in porous rock – A review, Geophysics**: 75**, 75A147 – 75A164.

Pride, S.R., A. F. Gangi, and F.D. Morgan, 1992. Deriving the equations of motion for porous isotropic media: J. Acoust. Soc. Am., **92** (6), 3278–3290.

Pride,S. R., and J.G. Berryman, 2003. Linear dynamics of double-porosity dual-permeability materials. I. Governing equations and acoustic attenuation: Phys. Rev. E, **68**, 036603.

Pride, S. R., E. Tromeur, and J. G. Berryman, 2002. Biot slow-wave effects in stratified rock: Geophysics, **67**(1), 271–281, doi: 10.1190/1.1451799.

Ricker N., 1941. A note on the determination of the viscosity of shale from the measurement of wavelet breadth: Geophysics, **6**, 254–258.

Rubino, J. G., and K. Holliger, 2012. Seismic attenuation and velocity dispersion in heterogeneous partially saturated porous rock: Geophysical Journal International, **188**, 1088–1102, doi: 10.1111/j.1365-246X.2011.05291.x

Spencer, J. W., Jr., 2013. Viscoelasticity of Ells River bitumen sand and 4D monitoring of thermal enhanced oil recovery processes: Geophysics, **78** (6), D419–D428, doi: 10.1190/GEO2012-0535.1

Tisato N. and C. Madonna, 2012. Attenuation at low seismic frequencies in partially saturated rocks: Measurements and description of a new apparatus: Journal of Applied Geophysics **86**, 44-53.

Tschoegl, N.W., Knauss ,W., & Emri, I., 2002. Poisson's ratio in linear viscoelasticity – a critical review: Mech. Time-Depend. Mater. **6**, 3–51

Toms, J., T. M. Müller, R. Ciz, and B. Gurevich, 2006. Comparative review of theoretical models of elastic wave attenuation and dispersion in partially saturated rocks: Soil Dynamics and Earthquake Engineering, **26**, 548-565.

White, J. E., 1965. Reflections from lossy media, J. Acoust. Soc. Am., 38, 604–607.

White, J. E., 1975. Computed seismic speeds and attenuation in rocks with partial gas saturation, Geophysics, **40** (2), 224–232.

White, J. E., 1986. Biot-Gardner theory of extensional waves in porous rods: Geophysics, **51**(3), 742-745.

Wong, J., and Lines, L., 2013. Physical modelling of reflections from low-*Q* media: Canadian Journal of Exploration Geophysics, **38**, 32-39

Zhu, T., J. M. Carcione, and J.M. Harris, 2013, Approximating constant-*Q* seismic propagation in the time domain: Geophysical Prospecting, **61**, 931 – 940, doi: 10.1111/1365-2478.12044.

Tables

Table 1. Physical parameters of brine- and gas-saturated sand used in the examples (after Dutta and Odé (1979b)

	Rock	
V_P	1500 m/s	P-wave velocity of dry matrix
V_S	1000 m/s	S-wave velocity of dry matrix
K_s	35 GPa	Bulk modulus of solid grains
ρ_s	2650 kg/m^3	Density of solid grains
ϕ	0.3	Porosity
κ	$9.869233 \cdot 10^{-13}$ (1 Darcy)	Permeability
a	1	Tortuosity
	Brine	
K_{fl}	2.4 GPa	Bulk modulus
ρ_{fl}	1000 kg/m^3	Density
η	$1 \cdot 10^{-3}$	Viscosity
	Gas	
K_{fl}	0.0022 GPa	Bulk modulus
ρ_{fl}	100 kg/m^3	Density
η	$1.5 \cdot 10^{-5}$	Viscosity

Figures

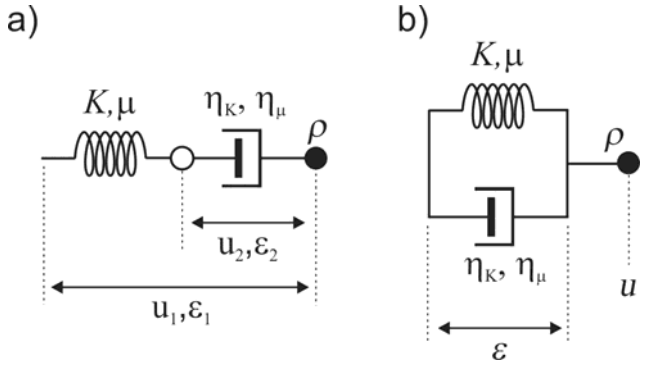

Figure 1. Spring-dashpot diagram of: a) Maxwell medium, b) Kelvin-Voigt medium. Black dots indicate the observable variable (displacement), $\mathbf{u}_1$, with the corresponding spatial derivative (strain, $\boldsymbol{\varepsilon}_1$). White dot is the internal variable, $\mathbf{u}_2$, and the corresponding strain is $\boldsymbol{\varepsilon}_2$. The spring denotes both bulk and shear elasticity, and the dashpot similarly represents both types of linear viscous friction.

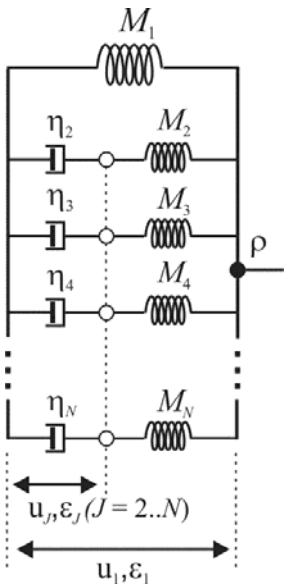

Figure 2. Generalized Standard Linear Solid commonly used in finite-difference modeling of seismic waves in VE media. Variable u_1 and its gradients ε_1 represent the observable variable, and variables $\mathbf{u}_J$ ($J = 2 \ldots N$) are the internal variables added to implement band-limited attenuation (Liu et al., 1976). With $N = 2$, this model represents the Standard Linear Solid.

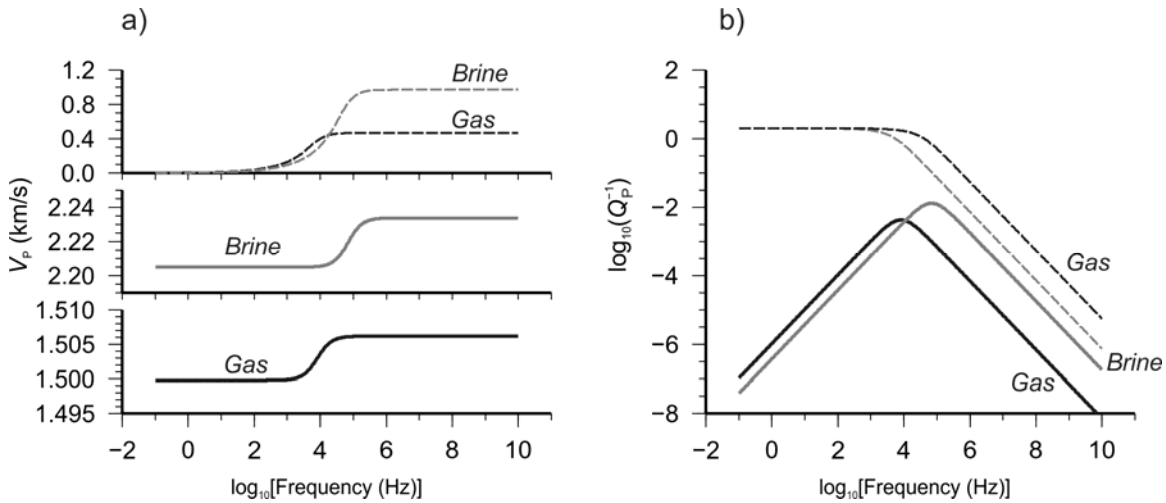

Figure 3. Properties of P waves in uniform brine- and gas-saturated sandstone (Table 1): a) Phase velocities; b) Attenuation factors. Black lines correspond to brine-saturated rock, gray lines – to gas-saturated rock. Solid lines correspond to the primary modes, dashed lines are the Biot's (1962) slow modes.

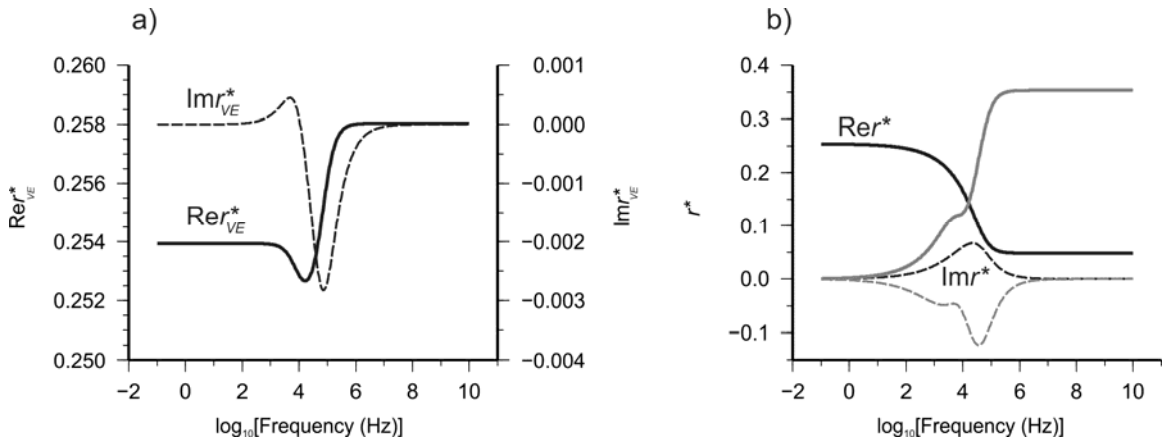

Figure 4. Reflection coefficients from a boundary between zones saturated with brine and gas (solid black lines – Rer^*, dashed black lines – Imr^*): a) Evaluated using the viscoelastic effective moduli; b) The solution from poroelasticity. Gray lines in plot b) show the respective conversion amplitudes to the reflected slow mode. Note that the two models are close at low frequencies, qualitatively similar up to frequencies of ~10^4 Hz, and completely dissimilar at higher frequencies.

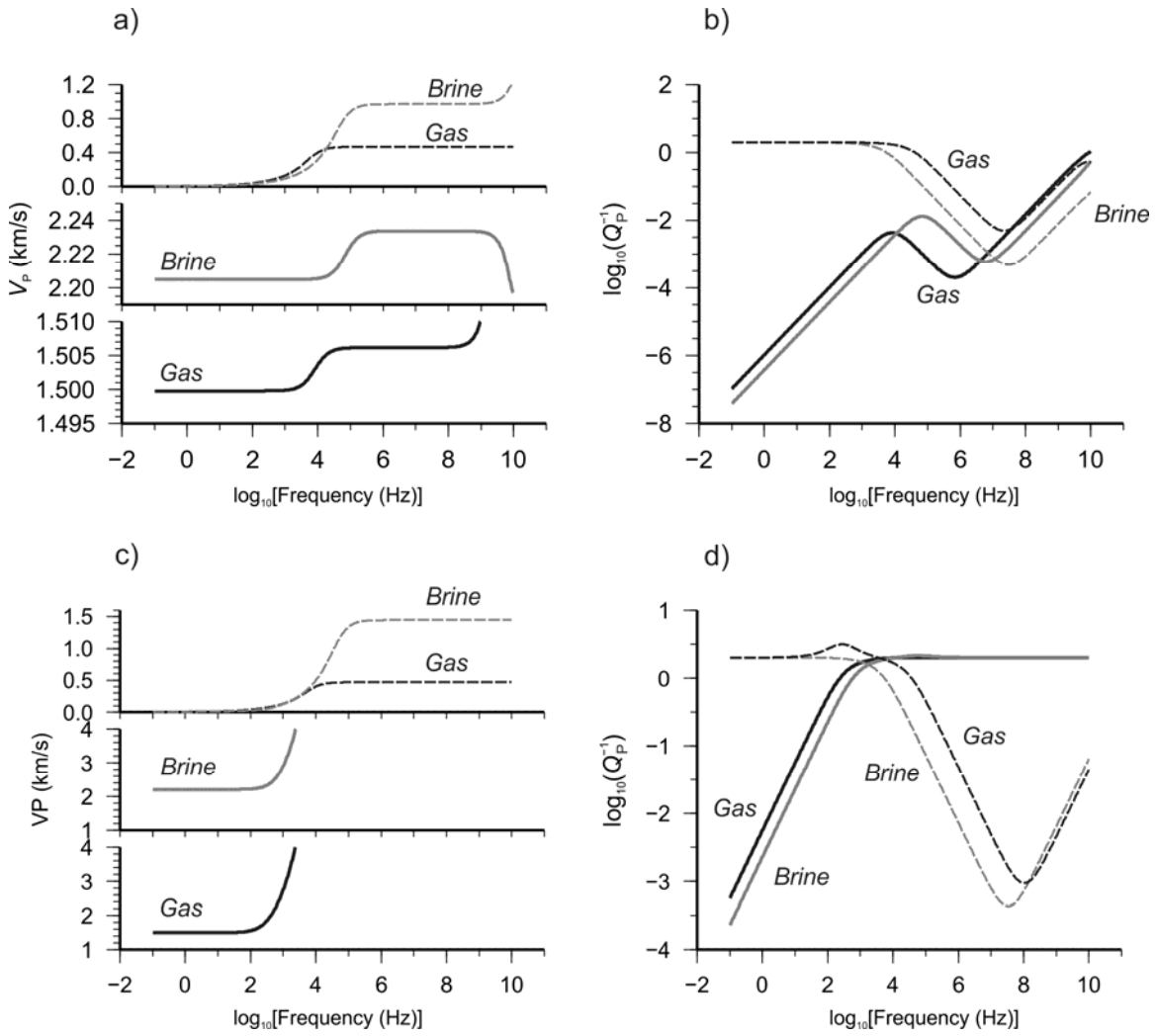

Figure 5. P-wave propagation in fluid-saturated media (Table 1) with bulk solid viscosity. The labels and line styles are as in Figure 3. a) Phase velocities for $\eta_M = 0.1$Pa·s in equation 29; b) Attenuation factors for this η_M; c) and d) are the same for $\eta_M = 3.8 \cdot 10^6$ Pa·s. Black lines correspond to brine—saturated rock, gray lines – to gas-saturated rock. Solid lines correspond to the primary modes, dashed lines show Biot's slow modes.

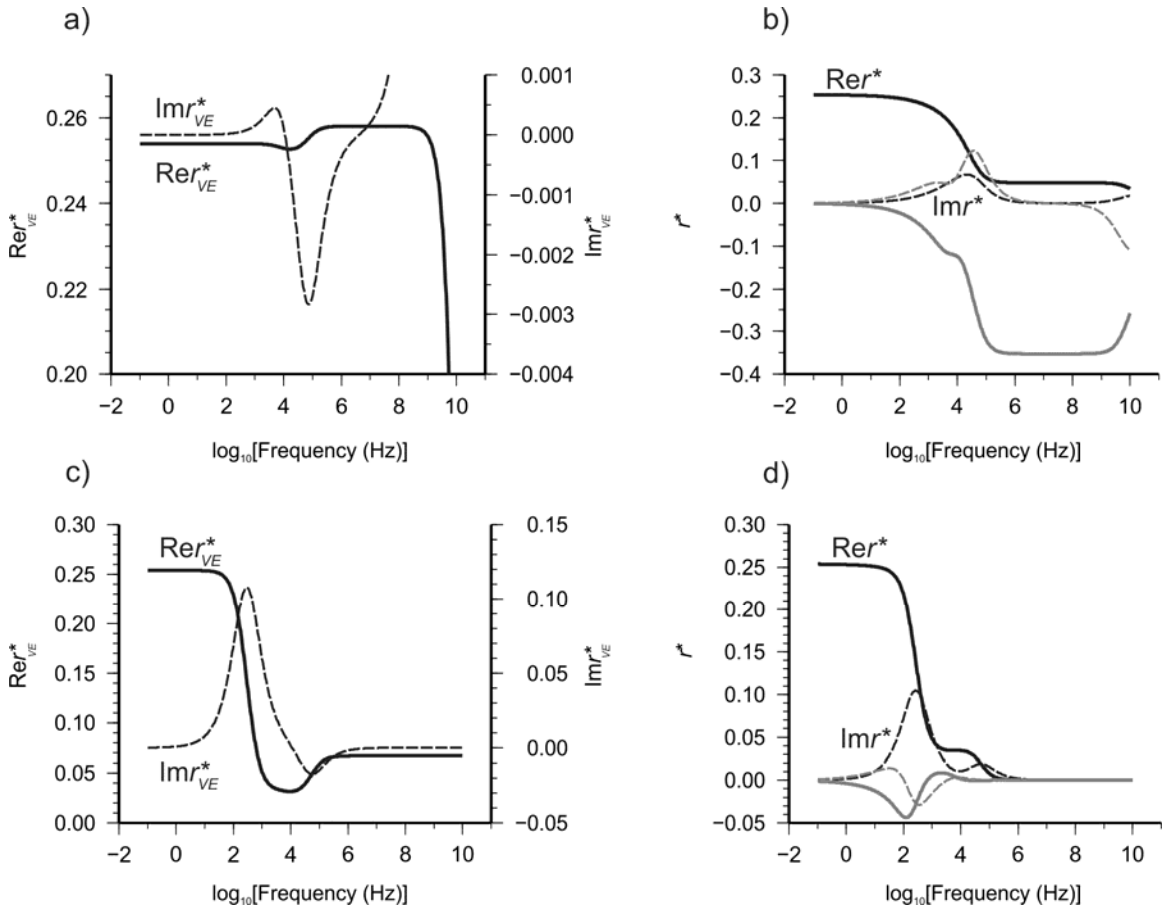

Figure 6. Reflection coefficients as in Figure 4 but with additional rock- and fluid P-wave viscosities: a) Solution based on the effective viscoelastic moduli inferred from the GLS model with $\eta_M = 0.1$Pa·s (equation 29); b) Reflectivity in the full GLS model (equation 15) with the same η_M; c) and d) are the same for $\eta_M = 3.8 \cdot 10^6$ Pa·s. In plot d), the mode conversion amplitudes (gray lines) are multiplied by 100.

Appendix A: Energy equipartitioning, diffusion, and skin layers

For a selected eigenmode $\boldsymbol{\upsilon}^{(n)} \equiv \boldsymbol{\upsilon}$ (here we drop the superscript for brevity), equation 15 in the text gives a relation between the average elastic energy $\left\langle \boldsymbol{\upsilon}^{+}\mathbf{M}\boldsymbol{\upsilon} \right\rangle$, kinetic energy $\left\langle \boldsymbol{\upsilon}^{+}\boldsymbol{\rho}\boldsymbol{\upsilon} \right\rangle$, viscous dissipation $\left\langle \boldsymbol{\upsilon}^{+}\boldsymbol{\eta}\boldsymbol{\upsilon} \right\rangle$, and Darcy-type frictional dissipation $\left\langle \boldsymbol{\upsilon}^{+}\mathbf{d}\boldsymbol{\upsilon} \right\rangle$:

$$\left(k+i\alpha\right)^{2}\left(\left\langle \boldsymbol{\upsilon}^{+}\mathbf{M}\boldsymbol{\upsilon} \right\rangle - i\omega\left\langle \boldsymbol{\upsilon}^{+}\boldsymbol{\eta}\boldsymbol{\upsilon} \right\rangle\right) = \omega^{2}\left\langle \boldsymbol{\upsilon}^{+}\boldsymbol{\rho}\boldsymbol{\upsilon} \right\rangle + i\omega\left\langle \boldsymbol{\upsilon}^{+}\mathbf{d}\boldsymbol{\upsilon} \right\rangle, \tag{A1}$$

where $\boldsymbol{\upsilon}^{+} \equiv \overline{\boldsymbol{\upsilon}}^{T}$ denotes the Hermitian conjugate. In several limiting cases, this relation gives useful energy relations within the wave:

1) For negligible energy dissipation ($\boldsymbol{\eta} \approx \mathbf{0}$ and $\mathbf{d} \approx \mathbf{0}$), the kinetic and elastic energies in a propagating wave are equal (*energy equipartitioning*; Aki and Richards, 2002): $\left(k+i\alpha\right)^{2}\left\langle \boldsymbol{\upsilon}^{+}\mathbf{M}\boldsymbol{\upsilon} \right\rangle = \omega^{2}\left\langle \boldsymbol{\upsilon}^{+}\boldsymbol{\rho}\boldsymbol{\upsilon} \right\rangle$, and therefore:

$$\left(k+i\alpha\right)^{2} = \omega^{2}\frac{\left\langle \boldsymbol{\upsilon}^{+}\boldsymbol{\rho}\boldsymbol{\upsilon} \right\rangle}{\left\langle \boldsymbol{\upsilon}^{+}\mathbf{M}\boldsymbol{\upsilon} \right\rangle}. \tag{A2}$$

This gives the standard relation for wave speed: $V_{\text{phase}} \equiv \omega/k = \sqrt{\left\langle \boldsymbol{\upsilon}^{+}\mathbf{M}\boldsymbol{\upsilon} \right\rangle / \left\langle \boldsymbol{\upsilon}^{+}\boldsymbol{\rho}\boldsymbol{\upsilon} \right\rangle}$.

2) For viscosity forces dominant over all others ($\mathbf{M} \approx \mathbf{0}$ and $\mathbf{d} \approx \mathbf{0}$), the wave is diffusive, with complex wavenumber:

$$\left(k+i\alpha\right)^{2} = i\omega\frac{\left\langle \boldsymbol{\upsilon}^{+}\boldsymbol{\rho}\boldsymbol{\upsilon} \right\rangle}{\left\langle \boldsymbol{\upsilon}^{+}\boldsymbol{\eta}\boldsymbol{\upsilon} \right\rangle}. \tag{A3}$$

This relation describes a 'skin layer' within the material, with the wavenumber and logarithmic amplitude decrement being equal each other (Landau and Lifshitz, 1987):

$$\alpha = k = \sqrt{\omega}\sqrt{\left\langle \boldsymbol{\upsilon}^{+}\boldsymbol{\rho}\boldsymbol{\upsilon} \right\rangle / 2\left\langle \boldsymbol{\upsilon}^{+}\boldsymbol{\eta}\boldsymbol{\upsilon} \right\rangle}. \tag{A4}$$

The thickness of the skin layer decreases with frequency:

$$\delta = 1/\alpha \propto 1/\sqrt{\omega}. \tag{A5}$$

3) For low viscosity and low frequency ($\boldsymbol{\eta} \approx \mathbf{0}$ and $\omega\left\langle \boldsymbol{\upsilon}^{+}\boldsymbol{\rho}\boldsymbol{\upsilon} \right\rangle \ll \left\langle \boldsymbol{\upsilon}^{+}\mathbf{d}\boldsymbol{\upsilon} \right\rangle$, as in poroelasticity), a similar diffusion equation is obtained from Darcy's law:

$$\left(k+i\alpha\right)^{2} = i\omega\frac{\left\langle \boldsymbol{\upsilon}^{+}\mathbf{d}\boldsymbol{\upsilon} \right\rangle}{\left\langle \boldsymbol{\upsilon}^{+}\mathbf{M}\boldsymbol{\upsilon} \right\rangle}. \tag{A6}$$

Appendix B: Transmission and reflection of multi-modal wavefields in layered structures

We model the wave propagation and reflections in a stack of multiple layers by using the propagator-matrix method by (Kenentt and Kerry, 1979). This method was also used by Pride et al. (2002). Consider a time-harmonic wavefield at frequency ω that is common to all layers. Within each layer, denote A_1 and A_2 the amplitudes of the two wave eigenmodes and denote k_1 and k_2 their complex wavenumbers from equation 15. Let us use the superscripts '+' and '−' for the waves traveling in the positive and negative directions of axis X, respectively. With this notation, the wavefield at the rear boundary of each layer is represented by a four-component vector $\mathbf{q}_r = \left(A_1^+ \quad A_2^+ \quad A_1^- \quad A_2^-\right)^T$. At the front of the layer, the amplitudes are $\mathbf{q}_f = \mathbf{P}\mathbf{q}_r$, where $\mathbf{P}$ is the 'propagator' matrix:

$$\mathbf{P} = \begin{bmatrix} e^{ik_1 x} & 0 & 0 & 0 \\ 0 & e^{ik_2 x} & 0 & 0 \\ 0 & 0 & e^{-ik_1 x} & 0 \\ 0 & 0 & 0 & e^{-ik_2 x} \end{bmatrix}. \tag{B1}$$

Let us also denote $\mathbf{U}$ the matrix relating the eigenmode amplitudes to the displacements on the rear and front boundaries, respectively:

$$\mathbf{u}_{r,f} = \mathbf{U}\mathbf{q}_{r,f}, \text{ where } \mathbf{U} \equiv \begin{bmatrix} \boldsymbol{\upsilon}_1^{(1)} & \boldsymbol{\upsilon}_1^{(2)} & -\boldsymbol{\upsilon}_1^{(1)} & -\boldsymbol{\upsilon}_1^{(2)} \\ \boldsymbol{\upsilon}_2^{(1)} & \boldsymbol{\upsilon}_2^{(2)} & -\boldsymbol{\upsilon}_2^{(1)} & -\boldsymbol{\upsilon}_2^{(2)} \end{bmatrix}. \tag{B2}$$

The negative signs for the backward-traveling modes correspond to the usual convention about the positive direction of particle motion P-wave being the direction of wave propagation. For the elastic and viscous stresses on the boundaries, we can similarly define matrix $\boldsymbol{\Sigma}$ from equations 13:

$$\boldsymbol{\sigma}_{r,f} = \boldsymbol{\Sigma}\mathbf{q}_{r,f}, \text{ where } \boldsymbol{\Sigma} \equiv i\left(\mathbf{M} - i\omega\boldsymbol{\eta}_M\right)\begin{bmatrix} k_1\boldsymbol{\upsilon}_1^{(1)} & k_2\boldsymbol{\upsilon}_1^{(2)} & k_1\boldsymbol{\upsilon}_1^{(1)} & k_2\boldsymbol{\upsilon}_1^{(2)} \\ k_1\boldsymbol{\upsilon}_2^{(1)} & k_2\boldsymbol{\upsilon}_2^{(2)} & k_1\boldsymbol{\upsilon}_2^{(1)} & k_2\boldsymbol{\upsilon}_2^{(2)} \end{bmatrix}. \tag{B3}$$

We can then combine the displacements and stresses in a single boundary-condition matrix $\mathbf{B}$:

$$\begin{bmatrix} \mathbf{u}_{r,f} \\ \boldsymbol{\sigma}_{r,f} \end{bmatrix} = \mathbf{B}\mathbf{q}_{r,f}, \text{ where } \mathbf{B} = \begin{bmatrix} \mathbf{U} \\ \boldsymbol{\Sigma} \end{bmatrix}. \tag{B4}$$

The boundary condition between the layers requires continuity of both displacement and stress. Let us assume that the fluid can freely flow across the boundary, which means that the pore pressure is also continuous. From relation B4, this boundary condition for layers 1 and 2 is:

$$\mathbf{B}^1\mathbf{q}_f^1 = \mathbf{B}^2\mathbf{q}_r^2, \tag{B5}$$

where the superscripts 'j' are the layer numbers. The case of an impermeable boundary between the layers ($u_2^1 = u_2^2 = 0$) can be treated analogously and shows a distinctly different behavior (Part II).

Using this boundary condition between layers $j = 1$ (brine) and $j = 2$ (gas), we can express $\mathbf{q}_f^1$ through the field in the next layer: $\mathbf{q}_f^1 = \tilde{\mathbf{B}}\mathbf{q}_r^2$, where $\tilde{\mathbf{B}} \equiv \left(\mathbf{B}^1\right)^{-1}\mathbf{B}^2$. Let us consider a wavefield traveling in both directions within layer 1: $\mathbf{q}_f^1 = \left(\mathbf{A}^{1+} \quad \mathbf{A}^{1-}\right)^T$ but only forward within layer 2: $\mathbf{q}_r^2 = \left(\mathbf{A}^{2+} \quad \mathbf{0}\right)^T$, where superscripts '+' and '–' denote the modes traveling forward and backward, respectively. By partitioning the matrix $\tilde{\mathbf{B}}$ into 2×2 blocks, we have:

$$\begin{bmatrix} \mathbf{A}^{1+} \\ \mathbf{A}^{1-} \end{bmatrix} = \begin{bmatrix} \mathbf{B}^{++} & \mathbf{B}^{+-} \\ \mathbf{B}^{-+} & \mathbf{B}^{--} \end{bmatrix} \begin{bmatrix} \mathbf{A}^{2+} \\ \mathbf{0} \end{bmatrix}. \tag{B6}$$

From the first row of this equation, we obtain: $\mathbf{A}^{2+} = \left(\mathbf{B}^{++}\right)^{-1}\mathbf{A}^{1+}$, meaning that the (matrix) transmission coefficient equals $\mathbf{T} = \left(\mathbf{B}^{++}\right)^{-1}$. The forward- and backward-traveling modes within layer 1 should be related by the reflection matrix $\mathbf{R}$ as $\mathbf{A}^{1-} = \mathbf{R}\mathbf{A}^{1+}$, and therefore:

$$\mathbf{R} = \mathbf{B}^{-+}\left(\mathbf{B}^{++}\right)^{-1} = \mathbf{B}^{-+}\mathbf{T}. \tag{B7}$$

Matrix $\mathbf{R}$ contains all reflection and mode-conversion coefficients on the boundary.